challenge in the study of recombination. A population sequencing approach, such as the one taken here, should enable further informative studies of recombination across a wide range of species.

References and Notes

1. G. Coop, M. Przeworski, *Nat. Rev. Genet.* **8**, 23 (2007).
2. S. Myers *et al.*, *Science* **327**, 876 (2010).
3. S. E. Ptak *et al.*, *Nat. Genet.* **37**, 429 (2005).
4. S. E. Ptak *et al.*, *PLoS Biol.* **2**, e155 (2004).
5. W. Winckler *et al.*, *Science* **308**, 107 (2005).
6. J. D. Wall, L. A. Frisse, R. R. Hudson, A. Di Rienzo, *Am. J. Hum. Genet.* **73**, 1330 (2003).
7. F. Baudat *et al.*, *Science* **327**, 836 (2010).
8. E. D. Parvanov, P. M. Petkov, K. Paigen, *Science* **327**, 835 (2010).
9. C. Grey *et al.*, *PLoS Biol.* **9**, e1001176 (2011).
10. P. L. Oliver *et al.*, *PLoS Genet.* **5**, e1000753 (2009).
11. I. L. Berg *et al.*, *Nat. Genet.* **42**, 859 (2010).
12. I. L. Berg *et al.*, *Proc. Natl. Acad. Sci. U.S.A.* **108**, 12378 (2011).
13. A. G. Hinch *et al.*, *Nature* **476**, 170 (2011).
14. S. Myers, L. Bottolo, C. Freeman, G. McVean, P. Donnelly, *Science* **310**, 321 (2005).
15. A. Kong *et al.*, *Nature* **467**, 1099 (2010).
16. International HapMap Consortium, *Nature* **449**, 851 (2007).
17. F. Smagulova *et al.*, *Nature* **472**, 375 (2011).
18. E. Mancera, R. Bourgon, A. Brozzi, W. Huber, L. M. Steinmetz, *Nature* **454**, 479 (2008).
19. J. Pan *et al.*, *Cell* **144**, 719 (2011).
20. G. A. McVean *et al.*, *Science* **304**, 581 (2004).
21. M. P. Stumpf, G. A. McVean, *Nat. Rev. Genet.* **4**, 959 (2003).
22. 1000 Genomes Project Consortium, *Nature* **467**, 1061 (2010).
23. Detailed information on methods and analyses can be found in the supplementary materials available in *Science* Online.
24. J. W. IJdo, A. Baldini, D. C. Ward, S. T. Reeders, R. A. Wells, *Proc. Natl. Acad. Sci. U.S.A.* **88**, 9051 (1991).
25. S. Myers, C. Freeman, A. Auton, P. Donnelly, G. McVean, *Nat. Genet.* **40**, 1124 (2008).
26. V. R. Ramirez-Carrozzi *et al.*, *Cell* **138**, 114 (2009).
27. T. D. Petes, *Nat. Rev. Genet.* **2**, 360 (2001).
28. J. L. Caswell *et al.*, *PLoS Genet.* **4**, e1000057 (2008).
29. A. V. Persikov, M. Singh, *Phys. Biol.* **8**, 035010 (2011).
30. C. C. Spencer *et al.*, *PLoS Genet.* **2**, e148 (2006).
31. S. Katzman, J. A. Capra, D. Haussler, K. S. Pollard, *Genome Biol. Evol.* **3**, 614 (2011).
32. T. R. Dreszer, G. D. Wall, D. Haussler, K. S. Pollard, *Genome Res.* **17**, 1420 (2007).
33. K. Paigen, P. Petkov, *Nat. Rev. Genet.* **11**, 221 (2010).
34. E. Axelsson, M. T. Webster, A. Ratnakumar, C. P. Ponting, K. Lindblad-Toh; LUPA Consortium, *Genome Res.* **22**, 51 (2012).

Acknowledgments: This work was funded by NIH grants R01 GM83098 (to M.P.) and T32 GM007197 (to E.M.L.) and by Wellcome Trust grants 076113/E/04/Z (to P.D.), 086084/Z/08/Z (to G.M.), and 090532/Z/09/Z contribution to Core Facility. P.D. was supported in part by a Wolfson-Royal Society Merit Award. M.P. is supported by the Howard Hughes Medical Institute. O.V. is funded by a Wellcome Trust studentship (086786/Z/08/Z). We thank G. Sella, G. McVicker, members of the PPS labs, and reviewers for their comments and H. Thorogood and W. Czyz for assistance with *PRDM9* sequencing. Part of this work has been supported by EUPRIM-Net under the European Union contract RII3-026155 of the 6th Framework Programme. Data are available from http://panmap.uchicago.edu. Some primate samples used in this study are under a Material Transfer Agreement from the San Diego Zoo.

Supplementary Materials

www.sciencemag.org/cgi/content/full/science.1216872/DC1
Materials and Methods
Figs. S1 to S21
Tables S1 to S9
References (*35*–*60*)

21 November 2011; accepted 27 February 2012
Published online 15 March 2012;
10.1126/science.1216872

REPORTS

Observation of Skyrmions in a Multiferroic Material

S. Seki,[1]* X. Z. Yu,[2] S. Ishiwata,[1] Y. Tokura[1,2,3]

A magnetic skyrmion is a topologically stable particle-like object that appears as a vortex-like spin texture at the nanometer scale in a chiral-lattice magnet. Skyrmions have been observed in metallic materials, where they are controllable by electric currents. Here, we report the experimental discovery of magnetoelectric skyrmions in an insulating chiral-lattice magnet Cu_2OSeO_3 through Lorentz transmission electron microscopy and magnetic susceptibility measurements. We find that the skyrmion can magnetically induce electric polarization. The observed magnetoelectric coupling may potentially enable the manipulation of the skyrmion by an external electric field without losses due to joule heating.

Topological spin textures in solids are of great interest to future spin-electronic technology. One example is a magnetic skyrmion (*1*–*3*), a vortex-like spin-swirling object (Fig. 1H) with a typical size of 10 to 100 nm, recently observed in chiral-lattice magnets (*4*–*7*). Conduction electron flow with low current density can drive skyrmion motion, which in turn gives rise to the transverse electromotive force (*8*–*10*). Such electric controllability, as well as its particle-like nature with nanometric size, points to potential application of skyrmions in high-density magnetic storage devices.

Another promising route to electric control of magnetism is through the usage of multiferroics, insulating materials characterized by both magnetic and dielectric orders (*11*). Recently, helical spin textures have been found to affect the symmetry of charge distribution and magnetically induce electric polarization (P) in compounds such as $TbMnO_3$ (*12*–*14*). Such coupling between ferroelectricity and magnetic structure enables versatile magnetoelectric response, such as the magnetic field (H) control of electric polarization direction (*14*) and the electric field (E) control of spin-chirality (*15*, *16*), magnetic modulation vector ($\vec{q}$) (*17*), and magnetic domain distribution (*18*). Because the energy dissipation by applied E is negligible in insulators, this approach is energetically more efficient compared with the current-driven approach in metals or semiconductors.

In the noncentrosymmetic environment of a chiral lattice, the spin-exchange interactions are composed of two terms: symmetric $\vec{S}_i \cdot \vec{S}_j$-like (e.g., ferromagnetic) and antisymmetric $\vec{S}_i \times \vec{S}_j$-like, where $\vec{S}_i$ and $\vec{S}_j$ represent spins on neighboring sites. The antisymmetric exchange term, called Dzyaloshinskii-Moriya (D-M) interaction, stems from the relativistic spin-orbit interaction and tends to stabilize helical (mostly screwlike) spin texture with fixed handedness (spin chirality) against the simple ferromagnetic state. The skyrmions or their crystallized form are known to appear in a restricted window of magnetic fields and temperatures in chiral-lattice helimagnets as the intervening state between the helical and field-induced spin-collinear (ferromagnetic) states. The crystallized form of skyrmions has been experimentally detected in specific metallic alloys with B20 structure, such as MnSi (*4*), $Fe_{1-x}Co_xSi$ (*5*, *6*), and FeGe (*7*). They all have a cubic crystal lattice with chiral space group $P2_13$, as well as the helimagnetic ground state formed as a result of the competition between the ferromagnetic exchange and D-M interactions (*19*). In bulk form, their magnetic phase diagram is characterized by the so-called A-phase, positioned within a narrow temperature (T) and magnetic field window just below the magnetic-ordering temperature (T_c) (*20*–*22*), where the formation of a triangular lattice of skyrmions is confirmed by small-angle neutron scattering experiments (*4*, *5*). In each skyrmion, spins at the core (or edge) of the vortex orient antiparallel (or parallel) to the applied H. The real-space observation of skyrmion crystal (SkX) by Lorentz transmission electron microscopy (TEM) has been

[1]Department of Applied Physics and Quantum Phase Electronics Center, University of Tokyo, Tokyo 113-8656, Japan. [2]Cross-Correlated Materials Research Group and Correlated Electron Research Group, RIKEN Advanced Science Institute, Wako 351-0198, Japan. [3]Multiferroics Project, Exploratory Research for Advanced Technology, Japan Science and Technology Agency, Tokyo 113-8656, Japan.

*To whom correspondence should be addressed. E-mail: seki@ap.t.u-tokyo.ac.jp

achieved for the thin-film form of the specimen (*6*, *7*), in which SkX is found to be stabilized over a much wider T and H range than in bulk specimen. Because the existence of the SkX state has been confirmed only in conductive materials (*4*, *5*, *7*), the dielectric nature of this spin state remains unexplored.

The crystal structure of Cu_2OSeO_3 is characterized by the same space group (cubic and chiral) $P2_13$ as the B20 alloys, but with very different atom coordination (Fig. 1A) (*23*–*25*). Cu^{2+} (spin $S = 1/2$) sites are surrounded by either a square pyramid or a trigonal bipyramid of oxygen ligands, with the ratio of 3:1. Recent powder neutron diffraction (*26*) and nuclear magnetic resonance (*27*) studies suggested that a three-up, one-down type of ferrimagnetic spin arrangement is realized in the magnetic ground state below $T_c \sim 60$ K, where collinear spins align antiparallel among two inequivalent Cu^{2+} sites (Fig. 1B). The single crystal of Cu_2OSeO_3 has been grown by chemical vapor transport method (*27*).

To investigate the nanometric-scale modification of the magnetic structure, we performed high-resolution Lorentz TEM imaging of a thin-film single crystal of Cu_2OSeO_3 with a thickness of ~100 nm. Combined with a magnetic transport-of-intensity equation calculation, this technique enables mapping the lateral magnetization distribution in real space (*28*). Under zero magnetic field for the (110) and (111) sample planes (Fig. 1, C and F, respectively), we observed the stripe patterns of the lateral magnetization, corresponding to a proper screw-spin order with a modulation period of ~50 nm, where spins rotate within a plane perpendicular to the magnetic modulation vector $q \parallel \langle 110 \rangle$. These results are consistent with the existence of a finite D-M interaction and reveal that the magnetic ground state of Cu_2OSeO_3 is helically modulated. Note that the modulation period (~50 nm) of the magnetic moment is long enough as compared with the Cu-Cu atomic distance, being compatible with the local ferrimagnetic spin arrangement. With $H \sim 800$ Oe applied normal to the sample plane, the formation of a triangular lattice of skyrmions is observed both for the (110) and (111) planes (Fig. 1, D and G). Here, the diameter of a skyrmion is identical to the modulation period of the helical spin state. Every skyrmion in the SkX state has a uniform spin chirality (spin-swirling direction), and three magnetic modulation vectors always lie perpendicular to the applied H. These features are consistent with the recent report for the SkX state in B20 alloys (*4*, *6*, *7*). Based on these real-space observations, Fig. 2B shows the H-T phase diagram under $H \parallel [111]$ for thin-film Cu_2OSeO_3 determined through the measurement of skyrmion density. Skyrmions disappear for $H > 1800$ Oe, which implies transition into the collinear (ferrimagnetic) spin state. Typical spin textures for selected (T, H) points are displayed in Fig. 2, D to K.

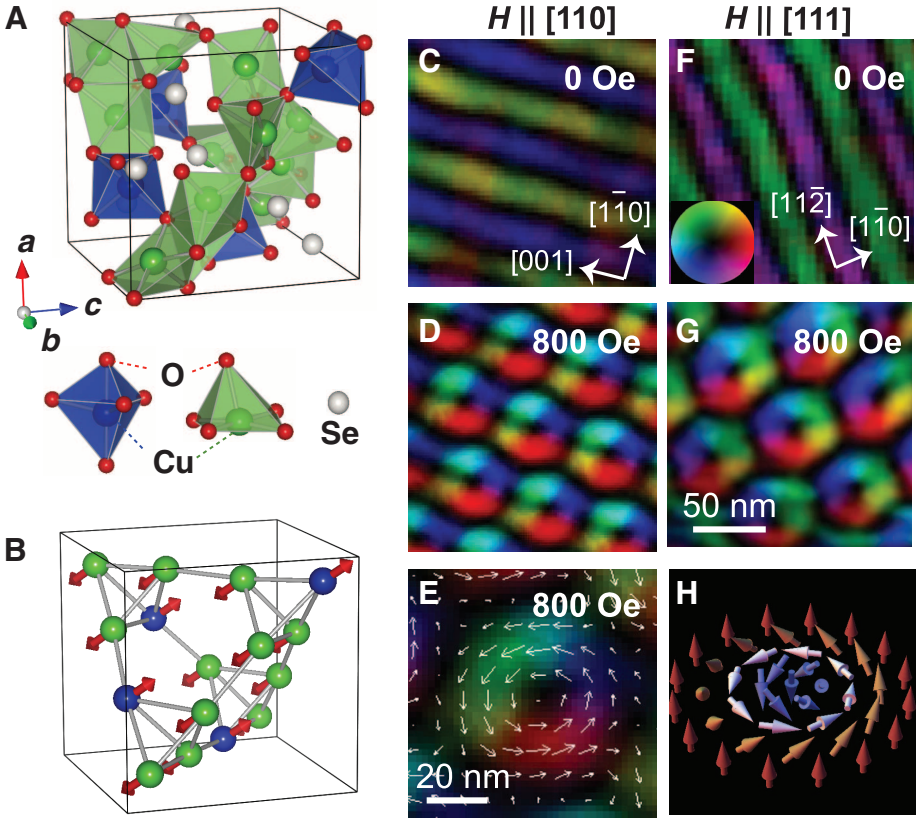

Fig. 1. (**A**) Crystal structure of Cu_2OSeO_3, characterized by two inequivalent Cu^{2+} sites with different oxygen coordination. (**B**) Ferrimagnetic spin arrangement on Cu^{2+} sites. (**C** to **G**) Lateral magnetization distribution map for a thin-film (~100-nm-thick) sample of Cu_2OSeO_3, obtained through the analysis of Lorentz TEM data taken at 5 K. The color wheel in the bottom-left corner of (F) shows the direction (hue) and relative magnitude (brightness) of the lateral magnetization. Panels (C) and (D), as well as (F) and (G), represent images for the (110) and (111) plane, respectively, and a magnetic field is applied normal to the observed sample plane. In both cases, proper screw-spin texture appears for zero magnetic field, whereas a skyrmion lattice with the identical spin chirality is formed for $H = 800$ Oe. A magnified view of (D) is shown in (E), where white arrows represent the magnetization direction. (**H**) Schematic illustration of a single magnetic skyrmion.

In B20 alloys, the stability of the SkX state essentially depends on the dimensions of the system: Whereas the SkX is stable over a wide T and H range in the two-dimensional (2D) limit (thin film), it shrinks into the narrow A-phase region in the 3D limit (bulk) (*6*, *7*). To investigate the effects of dimensionality in our system, we studied the magnetic behavior of a bulk single crystal of Cu_2OSeO_3 for $H \parallel [111]$. Figure 3, A and B, indicate the H-dependence of magnetization M and ac magnetic susceptibility χ' measured at 5 K. Around 600 Oe, the M profile shows a steplike anomaly, and χ' also exhibits a clear kink structure. Above 1800 Oe, M-value saturates at $M \sim 0.5\mu_B/Cu^{2+}$ (where μ_B is the Bohr magneton), which suggests the transition into the three-up, one-down ferrimagnetic state (Fig. 1B) (*25*, *26*, *29*). The same measurements are also performed at 55 (Fig. 3, D and E) and 57 K (Fig. 3, G and H), and the obtained χ' profiles indicate that the above two magnetic transitions still take place at both temperatures. Notably, we found an additional dip anomaly for 200 Oe $< H <$ 400 Oe in the χ' profile at 57 K, which has not been identified previously. The H-T phase diagram for the bulk crystal of Cu_2OSeO_3 obtained through H and T scans of M and χ' is summarized in Fig. 2, A and C. The overall features of the magnetic phase diagram, including the existence of a narrow A phase characterized by the dip anomaly in the χ' profile, bear close resemblance to those reported for B20 alloys (*21*, *30*). Considering the reported dimension dependence for the stability of the SkX state in B20 alloys (*6*, *7*), we conclude that the observed A phase represents the SkX state in the bulk form of Cu_2OSeO_3. The ground state of the bulk Cu_2OSeO_3 can be assigned to be helimagnetic, but with multiple q domains due to the high symmetry of the cubic lattice. Here, the application of H leads to the formation of a single q-domain state with $H \parallel q$ keeping the proper screw-spin texture, as antiferromagnetically aligned spins tend to lie perpendicular to the applied H. Such rearrangement of a q vector within the helimagnetic state explains the steplike anomaly of the M profile (Fig. 3A) and the enhancement of the χ' value (Fig. 3B) observed around 600 Oe at 5 K, as in the case of B20 (e.g., $Fe_{1-x}Co_xSi$) compounds (*22*).

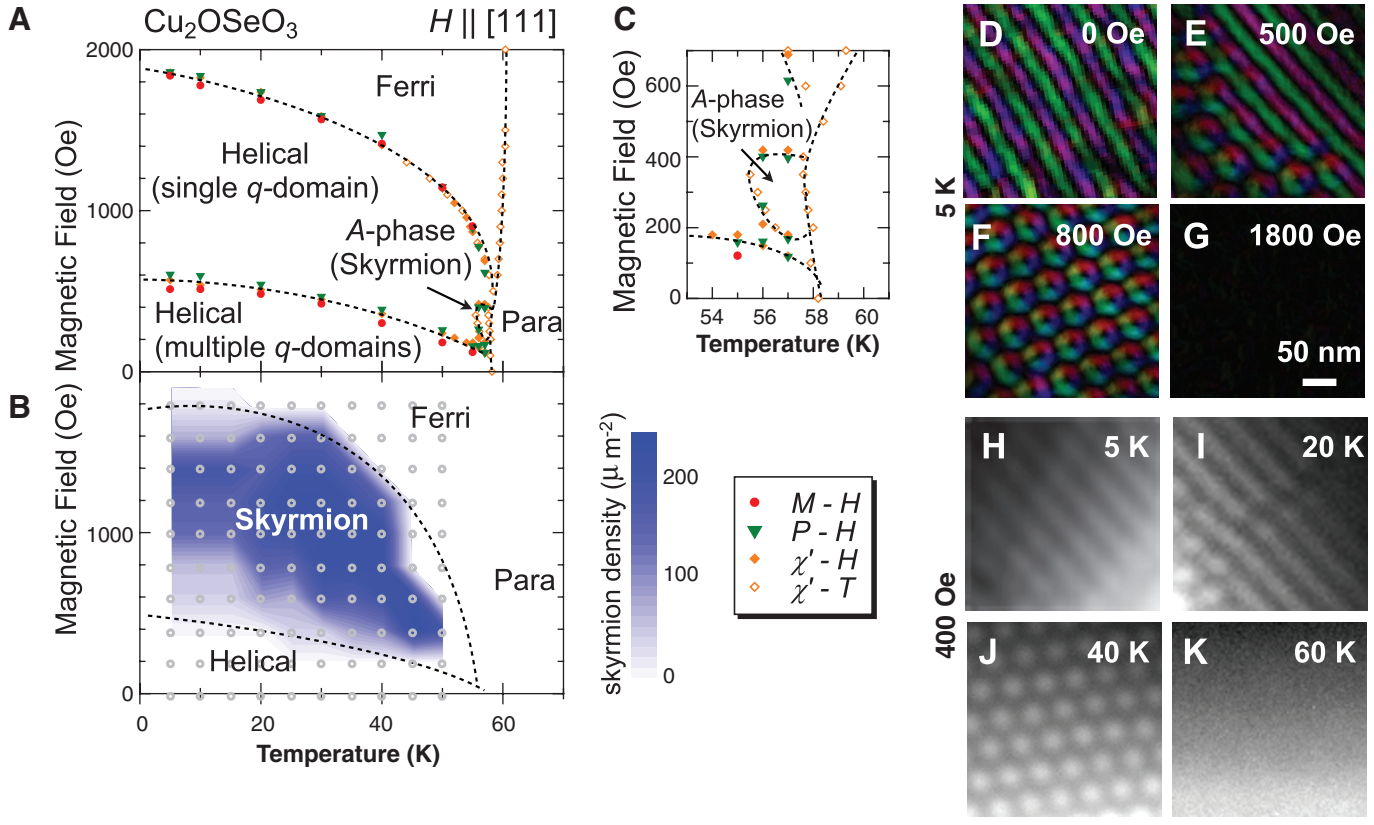

Fig. 2. Magnetic phase diagram under H || [111], deduced for (**A**) bulk and (**B**) thin-film forms of Cu_2OSeO_3, respectively. The former is determined by temperature (T) and magnetic-field (H) scans of magnetization (M), electric polarization (P), and ac magnetic susceptibility (χ'), and the latter by the measurement of skyrmion density through Lorentz TEM imaging at selected data points (small gray circles). (**C**) Magnified view of (A) near the A-phase (skyrmion crystal phase) region. (**D** to **G**) Magnetic field dependence of lateral magnetization distribution at 5 K with the same color wheel mapping as in Fig. 1, where a magnetic field is applied normal to the (111) thin film. (**H** to **K**) Temperature dependence of the magnetic domain configuration (underfocused Lorentz TEM images) with H = 400 Oe.

Cu_2OSeO_3 has recently been reported to show small anomalies in the dielectric constant accompanied with magnetic transitions (*26*, *31*). To fully understand the magnetoelectric response in this material, we performed the electric polarization measurement for each magnetic phase, focusing on the [111] component of the electric polarization ($P_{[111]}$) under H || [111]. Figure 3C indicates the magnetic field dependence of $P_{[111]}$ at 5 K, measured after cooling at zero E and H. In the helimagnetic phase with multiple q domains (denoted as h′), $P_{[111]}$ remains zero even under finite H (<400 Oe). Upon the transition into the single q-domain helimagnetic state (denoted as h) around 600 Oe, $P_{[111]}$ first takes a nonzero negative value but then changes its sign as H is further increased. In the ferrimagnetic state (denoted as f), $P_{[111]}$ saturates at a positive value. The reversal of the H direction gives the same sign as that of $P_{[111]}$. In general, application of H induces the continuous deformation of spin texture from proper screw to conical, and finally to collinear (that is, ferrimagnetic) (Fig. 4A). The variation of $P_{[111]}$ with H || [111] appears to be well scaled with the relation that $P_{[111]} = P_0 + \beta M^2$ (where P_0 and β are the fitting parameters) (red dashed line in Fig. 3C), except for the low-H region where P remains zero probably due to the cancelation of P averaged over different q domains.

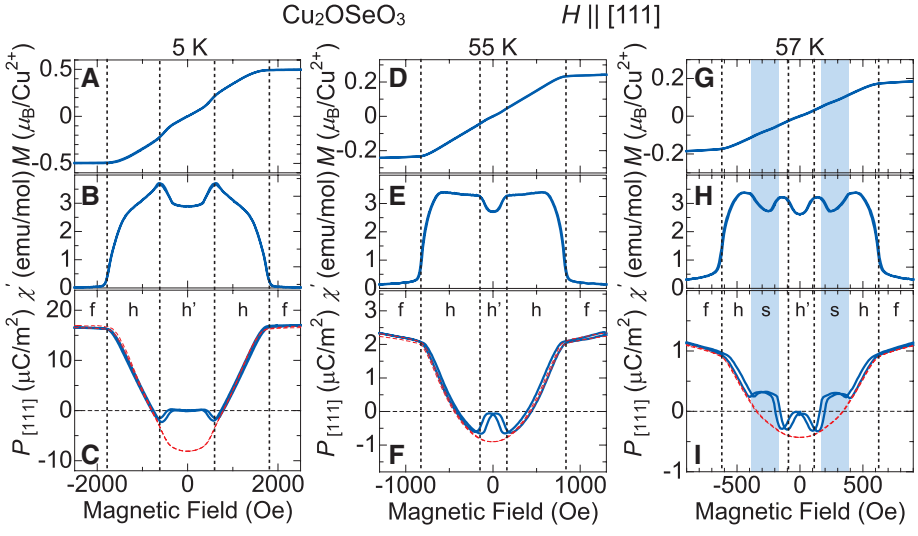

Fig. 3. Magnetic field (H || [111]) dependence of magnetization M, ac magnetic susceptibility χ', and [111]-component of electric polarization ($P_{[111]}$) measured for bulk single crystal of Cu_2OSeO_3 at 5 (**A** to **C**), 55 (**D** to **F**), and 57 K (**G** to **I**), respectively. Red dashed lines in the $P_{[111]}$-profiles indicate the numerical fit for the single-domain helimagnetic state with $P_{[111]} = P_0 + \beta M^2$. Letter symbols f, h, h′, and s denote ferrimagnetic, helimagnetic (single q domain), helimagnetic (multiple q domains), and skyrmion-crystal states, respectively.

Similar behavior is observed at elevated temperatures: 55 (Fig. 3F) and 57 K (Fig. 3I). However, when passing through the A phase—that is, the bulk SkX phase (denoted as s) at 57 K—$P_{[111]}$ shows an abrupt change and takes a nonzero positive value. Each magnetic transition

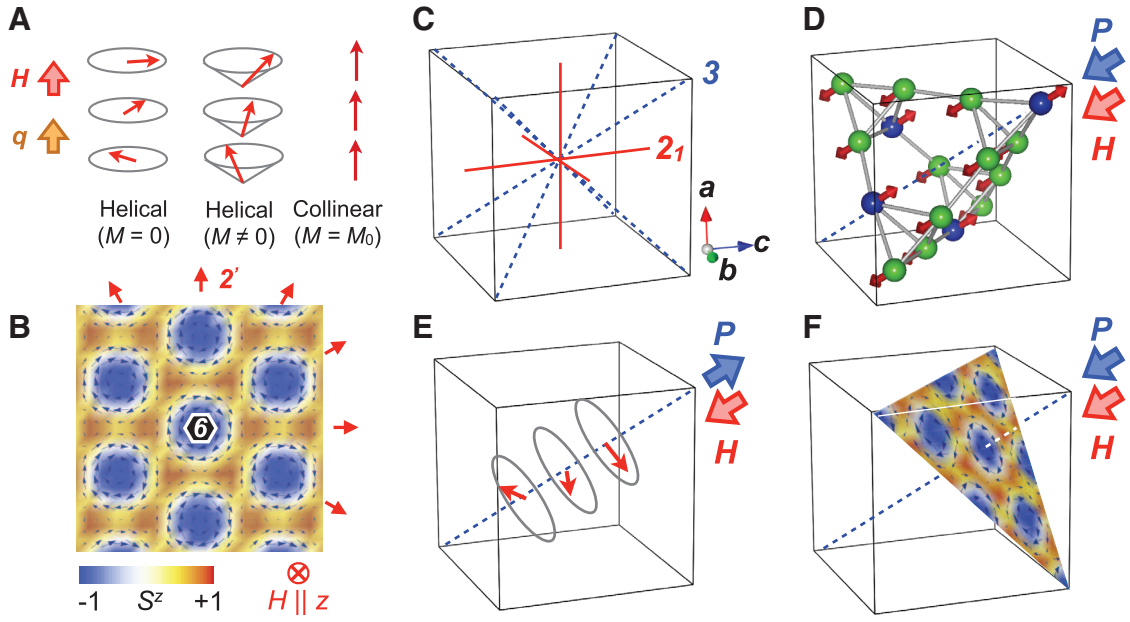

Fig. 4. (**A**) Development of helical spin order under an applied magnetic field. (**B**) Spin distribution for a magnetic skyrmion crystal, with background color representing the out-of-plane component of the magnetic moment (S^z). Compatible symmetry elements are also indicated: twofold rotation axes followed by time reversal (*2′*) and a sixfold rotation axis along the out-of-plane direction (*6*). Red arrows indicate 2′ axes. (**C**) Symmetry elements allowed for the crystal structure of Cu_2OSeO_3 with space group $P2_13$. (**D** to **F**) The *P* direction for ferrimagnetic, helimagnetic, and skyrmion-crystal states under $H \parallel [111]$, respectively.

coincides with the anomalies in the *P*-*H* profile (Fig. 2, A and C), suggesting a strong magnetoelectric coupling in this material. The above results indicate that all the magnetic phases (ferrimagnetic, helimagnetic, and even the skyrmion lattice spin state) can magnetically induce nonzero electric polarization with varying sign and magnitude.

The emergence of $P \parallel H \parallel [111]$ in these magnetic phases can be justified from the viewpoint of magnetic symmetry. The crystal structure of Cu_2OSeO_3 belongs to the nonpolar (paraelectric) space group $P2_13$, which possesses threefold rotation axes along <111> and 2_1-screw axes along <100> (Fig. 4C). The skyrmion lattice spin texture itself is also nonpolar, because it holds an orthogonal arrangement of a sixfold rotation axis (*6*) along *H* and twofold rotation axes followed by time reversal (*2′*) normal to *H* (Fig. 4B). When a skyrmion lattice is formed with $H \parallel [111]$ on the Cu_2OSeO_3 crystal lattice, however, most of symmetry elements are lost, and only the threefold rotation axis along the *H* direction survives. As a result, the system can become polar along the *H* direction, and the emergence of $P \parallel H \parallel [111]$ is allowed (Fig. 4F) (*32*). Likewise, the ferrimagnetic order with $H \parallel M \parallel [111]$ (Fig. 4D) or the helimagnetic order with $H \parallel q \parallel [111]$ (Fig. 4E) leaves only the threefold rotation axis or screw axis along *H*, and hence also allows the emergence of $P \parallel H \parallel [111]$. Because of the different magnetic-moment distributions, however, the *M* dependence of $P_{[111]}$ becomes distinct between the helimagnetic (conical) and SkX orders, thereby causing the nonmonotonous change of $P_{[111]}$ by way of the SkX state in the *H*-increasing/decreasing runs, as seen in Fig. 3I.

Cu_2OSeO_3 can be regarded as an insulating analog of B20 alloys, given the similarity in the crystal symmetry and a magnetic phase diagram characterized by the narrow A phase (SkX state) region; this might suggest that chiral-lattice cubic ferro/ferrimagnets ubiquitously host skyrmion spin texture regardless of metallic or insulating state. In insulators, the skyrmion can be accompanied by electric polarization, which may enable manipulation of skyrmions by an applied electric field. In B20 alloys (*6*), skyrmions can appear not only in crystallized form but also as independent particles, especially at the phase boundary between the collinear and SkX states. An individual skyrmion particle should locally carry a distinctive magnitude of electric dipole under the ferrimagnetic background in Cu_2OSeO_3, which, in principle, allows the transport of skyrmions by the spatial gradient of an electric field as the process of minimizing electrostatic energy. Skyrmions in multiferroics may be a building block to design energy-efficient spintronic devices with unique magnetoelectric functions.

References and Notes

1. T. H. R. Skyrme, *Nucl. Phys.* **31**, 556 (1962).
2. U. K. Rößler, A. N. Bogdanov, C. Pfleiderer, *Nature* **442**, 797 (2006).
3. A. N. Bogdanov, D. A. Yablonskii, *Sov. Phys. JETP* **68**, 101 (1989).
4. S. Mühlbauer *et al.*, *Science* **323**, 915 (2009).
5. W. Münzer *et al.*, *Phys. Rev. B* **81**, 041203(R) (2010).
6. X. Z. Yu *et al.*, *Nature* **465**, 901 (2010).
7. X. Z. Yu *et al.*, *Nat. Mater.* **10**, 106 (2011).
8. P. Bruno, V. K. Dugaev, M. Taillefumier, *Phys. Rev. Lett.* **93**, 096806 (2004).
9. A. Neubauer *et al.*, *Phys. Rev. Lett.* **102**, 186602 (2009).
10. F. Jonietz *et al.*, *Science* **330**, 1648 (2010).
11. M. Fiebig, *J. Phys. D Appl. Phys.* **38**, R123 (2005).
12. S. W. Cheong, M. Mostovoy, *Nat. Mater.* **6**, 13 (2007).
13. Y. Tokura, S. Seki, *Adv. Mater.* **22**, 1554 (2010).
14. T. Kimura *et al.*, *Nature* **426**, 55 (2003).
15. Y. Yamasaki *et al.*, *Phys. Rev. Lett.* **98**, 147204 (2007).
16. S. Seki *et al.*, *Phys. Rev. Lett.* **100**, 127201 (2008).
17. H. Murakawa, Y. Onose, Y. Tokura, *Phys. Rev. Lett.* **103**, 147201 (2009).
18. Y. Tokunaga *et al.*, *Nat. Mater.* **8**, 558 (2009).
19. Y. Ishikawa, K. Tajima, D. Bloch, M. Roth, *Solid State Commun.* **19**, 525 (1976).
20. Y. Ishikawa, M. Arai, *J. Phys. Soc. Jpn.* **53**, 2726 (1984).
21. A. Bauer *et al.*, *Phys. Rev. B* **82**, 064404 (2010).
22. S. V. Grigoriev *et al.*, *Phys. Rev. B* **76**, 224424 (2007).
23. G. Meunier, M. Bertaud, *J. Appl. Cryst.* **9**, 364 (1976).
24. H. Effenberger, F. Pertlik, *Monatsh. Chem.* **117**, 887 (1986).
25. K. Kohn, *J. Phys. Soc. Jpn.* **42**, 2065 (1977).
26. J.-W. G. Bos, C. Colin, T. Palstra, *Phys. Rev. B* **78**, 094416 (2008).
27. M. Belesi *et al.*, *Phys. Rev. B* **82**, 094422 (2010).
28. M. Uchida, Y. Onose, Y. Matsui, Y. Tokura, *Science* **311**, 359 (2006).
29. C. L. Huang *et al.*, *Phys. Rev. B* **83**, 052402 (2011).
30. C. Thessieu, C. Pfleiderer, A. N. Stepanov, J. Flouquet, *J. Phys. Condens. Matter* **9**, 6677 (1997).
31. K. H. Miller *et al.*, *Phys. Rev. B* **82**, 144107 (2010).
32. Based on the similar symmetry analysis, the emergence of $P \parallel [001]$ can be allowed in a skyrmion lattice spin state with $H \parallel [110]$, because only the $2_1'$-axis normal to *H* remains unbroken.

Acknowledgments: We thank N. Nagaosa, T. Arima, M. Mochizuki, S. Miyahara, N. Furukawa, B.-J. Yang, F. Kagawa, Y. Shiomi, N. Kanazawa, T. Kurumaji, M. Shibata, M. Rikiso, and A. Nakao for enlightening discussions and experimental contributions. This work was partly supported by Grants-In-Aid for Scientific Research (grants 20340086 and 2010458) from the Ministry of Education, Culture, Sports, Science and Technology of Japan, and the FIRST Program by the Japan Society for the Promotion of Science.

Supplementary Materials

www.sciencemag.org/cgi/content/full/336/6078/198/DC1
Materials and Methods
References

19 September 2011; accepted 2 March 2012
10.1126/science.1214143